Green Chemistry

PAPER

View Article Online
View Journal | View Issue

Cite this: *Green Chem.*, 2025, **27**, 9153

Medium ion-association electrolyte enables fast and stable K-storage for ferrocene-based organic anodes†

Jing Zheng, *[a] Qun Li,[a] Hao Wang,[a] Jijian Xu, *[b] Xiaokang Chu,[a] Ran Chen,[a] Haobo Xia,[c] Jianying Long,[a] Meng Lei,[a] Mengtao Ma, *[a] Zixia Lin[d] and Qingxue Lai*[c]

Received 19th April 2025,
Accepted 27th June 2025

DOI: 10.1039/d5gc01964h

rsc.li/greenchem

High-concentration electrolytes have demonstrated promise in improving the cycling stability of organic K-storage materials *via* suppressing dissolution of the organic active materials and enhancing interfacial stability. However, the improved cycling stability has been achieved at the expense of diminished K-storage kinetics. To overcome this challenge, herein, a green and environmentally friendly medium ion-association electrolyte (MIAE) with high ionic conductivity and anion-rich solvation structures was designed for organic ferrocene (Fc) K-storage anodes. The medium ion-association properties for the tailored solvation structures of MIAE can provide multiple benefits for fast and stable K-storage of Fc anodes *via* suppressing the dissolution of Fc, promoting the formation of a stable solid-electrolyte interphase (SEI), as well as accelerating the ion-transfer kinetics at the same time. As a result, the Fc anode in an ethylene carbonate (EC)-based MIAE delivered a reversible discharge capacity of 209.1 mAh g^{-1} after 200 cycles at 50 mA g^{-1} with an average coulombic efficiency (CE) of above 99.7%. This work provides valuable insights into the rational design of customized electrolytes for advanced organic potassium-ion batteries (PIBs).

Green foundation

1. Ferrocene (Fc), an eco-friendly material derived from abundant raw materials *via* a simple, low-waste synthesis process, has low toxicity and is biodegradable, and is utilized as an efficient organic anode for K-storage.
2. A medium ion-association electrolyte (MIAE), formulated with eco-friendly and per- and polyfluoroalkyl substance (PFAS)-free solvents, is developed to address the issues of unsatisfactory cycling stability and reaction kinetics of organic K-storage anodes.
3. The proposed green K-storage system of Fc||MIAE delivers a competitive K-storage performance when compared to previously reported organic K-storage anodes, demonstrating promising applications for organic potassium-ion batteries.

1. Introduction

Constructing reliable secondary energy storage batteries using renewable electrode materials is an effective solution to cater to the growing demand for electronics, energy equipment, and large-scale energy storage systems.[1,2] Potassium-ion batteries (PIBs) are a powerful alternative for sustainable energy storage devices based on their resource accessibility, cost-effective production, low K^+/K redox potential (−2.93 V compared to standard hydrogen electrodes), and charging/discharging mechanisms that are similar to standard commercial lithium-ion batteries.[3,4] However, rapid progress in research on PIBs remains severely hampered by the large ionic radius of K^+ (1.38 Å), making its insertion into electrode materials difficult in conventional battery systems. In particular, inorganic electrode materials are vulnerable to severe volume changes during cycling, leading to issues with low capacity and inferior cycling stability.[5,6] Organic redox-active materials with tunable molecular structures and soft lattice properties offer strategies to

[a]*Department of Chemistry and Materials Science, College of Science, Nanjing Forestry University, Nanjing 210037, P. R. China. E-mail: jzheng62@njfu.edu.cn, mengtao@njfu.edu.cn*
[b]*Department of Chemistry, City University of Hong Kong, Hong Kong 999077, China. E-mail: jijianxu@cityu.edu.hk*
[c]*Jiangsu Key Laboratory of Electrochemical Energy Storage Technologies, College of Materials Science and Technology, Nanjing University of Aeronautics and Astronautics, Nanjing 210016, P. R. China. E-mail: qx_lai@nuaa.edu.cn*
[d]*Testing Center, Yangzhou University, Yangzhou 225009, P. R. China*
† Electronic supplementary information (ESI) available. See DOI: https://doi.org/10.1039/d5gc01964h

improve the above problems.[7,8] In addition, organic materials have other advantages, including their environmental friendliness, low-cost properties, and flexible and versatile synthesis methods, which are prerequisites for the development of PIBs with high energy density and cost-effectiveness.[9,10]

To date, as described in a vast number of research articles, novel organic molecules with multiple redox-active sites, such as C═O, C═N, N═N and phenyl groups, have been extensively explored, alongside corresponding modifications of the resulting materials.[11,12] Unfortunately, these organic molecules still suffer from a series of disadvantages, including low electronic conductivity, easy solubility in organic electrolytes, and inefficient utilization of active sites in practical applications.[13] Ferrocene (Fc), which is a "sandwich" organometallic compound containing cyclopentadienyl anions on two sides of a divalent iron cation, exhibits excellent electrochemical responsiveness, thermal stability, and chemical resistance. Ferrocene reduces dependence on non-renewable resources and associated ecological damage caused by mining. Its synthesis reaction involves high utilization of raw materials and has fewer by-products, thus reducing wastage of resources.[14,15] According to a previous report, poly(vinyl ferrocene) containing Fc can function as an anion acceptor to extend the effective transportation of charge carriers and solve the issue of low ionic conductivity.[16] Metal–organic frameworks based on Fc with unique structures can act as highly stable K-storage anode materials *via* reducing the solubility problem of Fc in organic electrolytes.[15] In addition, Fc can also serve as an additive to improve reversibility and storage properties of conversion-type anode materials, inhibiting the clustering effect between molecules.[17] Meanwhile, Fc has been used as an anode material in lithium-ion batteries, and the discharge capacity can be stabilized at about 560 mAh g^{-1} after 100 cycles at 100 mA g^{-1} current density.[18] Although these Fc-based organic materials have demonstrated improved K-storage stability *via* molecular structure design, how to directly employ the commercial Fc molecules with cost-effective and easily accessible advantages as promising K-storage anode materials still remains a significant challenge.

Electrolyte engineering has been considered as an efficient strategy to enhance the K-storage performance of active materials, including improvements of properties such as the specific capacity, charging and discharging kinetics and cycling stability.[19,20] Generally, the occurrence of side reactions ultimately depends on the composition of K salts and organic solvents in the electrolyte, especially the relative proportions of free and solvated species and their interactions within the solvation sheath. A highly concentrated electrolyte (HCE) with limited amounts of free solvents and an anion-rich solvation sheath has been developed for active organic materials to achieve significantly improved cycling stability *via* suppression of the dissolution of active organic materials as well as the formation of a high-quality solid electrolyte interphase (SEI).[21–23] However, conventional HCEs usually exhibit significantly reduced ionic conductivity, primarily due to strong cation–anion associations that subsequently elevate dynamic viscosity and result in the inevitable sacrifice of K-storage kinetics.[24] Therefore, Fc organic anode materials are greatly required to design advanced electrolytes with highly matched thermodynamics and dynamics, and thus achieve stable and fast K-storage performance.

In this work, we proposed a medium ion-association electrolyte (MIAE) for a promising Fc-based organic K-storage anode. The Fc molecule with its redox-active iron group can provide stable K-storage sites. Besides, the conjugated system has enhanced conductivity with high delocalization of electrons.[25,26] In order to address the dissolution of the active material, an unstable interface and sluggish reaction kinetics, a range of electrolytes with tunable ion-association properties have been designed *via* rational manipulation of the solvent molecular structure and concentrations of salts. The optimized EC-based MIAE demonstrated high ion conductivity, anion-rich solvation structures with suppressed content of free solvents, as well as high compatibility with the Fc anode, providing a solid foundation for stable interfacial stability and fast reaction kinetics. At the same time, the use of this electrolyte significantly demonstrates non-fluorine and eco-friendly properties of low toxicity, low flammability, and low volatility, which are in line with the needs of green and sustainable development.[27] As a result, the Fc anode material in the optimized EC-based MIAE delivered a high specific capacity of 209.1 mAh g^{-1} at 50 mA g^{-1} for 200 cycles and a well-maintained specific capacity of 171.9 mAh g^{-1} after 200 cycles at 200 mA g^{-1} with an average CE of above 99.5%, thus providing a new pathway to customize well-matched electrolytes for advanced organic PIBs.

2. Experimental

2.1. Electrolyte preparation

Potassium bis(fluorosulfonyl)imide (KFSI) was obtained from J&K Scientific and utilized directly without any treatment. The solvents of ethylene carbonate (EC), dimethyl carbonate (DMC), propylene carbonate (PC) and vinylene carbonate (VC) were purchased from Sigma-Aldrich and applied after the removal of trace water using 4 Å molecular sieves. The as-prepared electrolytes were obtained by dissolving a certain molar mass of KFSI in EC + DMC ($V_1 : V_2 = 1 : 1$) or PC + DMC ($V_1 : V_2 = 1 : 1$) or VC + DMC ($V_1 : V_2 = 1 : 1$) solvents to formulate different electrolytes in an argon-filled glove box: 1 M KFSI/EC + DMC (abbreviated as LIAE); 3 M KFSI/EC + DMC (MIAE); 3 M KFSI/PC + DMC (PC-based MIAE); 3 M KFSI/VC + DMC (VC-based MIAE); and 5 M KFSI/EC + DMC (HIAE) ("M" equals $\text{molar}_{\text{salt}}/\text{litre}_{\text{solvent}}$).

2.2. Structural characterization

The solvation structures of the electrolytes were characterized using UV-visible spectrophotometry (UV-2700 spectrophotometer, Shimadzu), Fourier transform infrared (FTIR) spectroscopy (VERTEX 70, Bruker) and Raman spectroscopy (DXR532 instrument equipped with a 532 nm laser source,

Thermo Fisher Scientific). In addition, the safety of each electrolyte was assessed using a combustion test.

2.3. Coin cell assembly and electrochemical tests

The active material of ferrocene (Fc) was milled and a slurry was formed by mixing it for 30 min with Super P (a conductive additive) and polyvinylidene difluoride (PVDF, binder) in *N*-methylpyrrolidone (NMP) using mass ratio of 6 : 3 : 1. Then, the slurry was coated on aluminum (Al) foil and dried under vacuum at 60 °C for 12 h. The loading of Fc per unit area of Al foil was controlled to between 0.6 and 0.8 mg with a coating thickness was 100 μm. The prepared coated Al foil was cut into round electrodes of radius 6 mm and these were used as the working electrode, with potassium (K) foil used as the counter electrode and glass fiber (Whatman, GF/A) as the separator. CR2032-type coin cells were assembled from the prepared working electrode, counter electrode, separator and different electrolytes in an argon-filled glove box. Additionally, K||Cu and K||K cells were assembled under conditions similar to those mentioned above, except that the working electrodes were replaced respectively by Cu foil and K foil, while the separator was replaced with a different glass fiber (Whatman, GF/B).

Within the voltage range of 0.01 to 3.0 V, the galvanostatic charge/discharge (GDC) value and rate performance of the cells assembled using Fc were measured with a Neware battery test system (CT4008T) and Land battery test system (CT2001A). Besides, testing was also conducted using the galvanostatic intermittent titration technique (GITT) by charging and discharging the cell at 50 mA g^{-1} over the above voltage range, with the test program comprising 10 min for pulses and 1.0 h for relaxation. Cyclic voltammetry (CV) and electrochemical impedance spectroscopy (EIS) (0.01 Hz–100 kHz, 10 mV) tests were performed on an electrochemical workstation (CS2350H, Wuhan Corrtest Instruments) to evaluate K-storage properties. For K||Cu cells, the actual copper foil area (disc of 12 mm diameter) used to deposit K is 1.13 cm^2, which is discharged at a specific current density for 1.0 h, and then charging is continued at the above current density with a cutoff voltage of 3.0 V, and the above procedure is repeated *n* number of times. For K||K symmetric cells, the charge and discharge tests are conducted at specific current densities and fixed capacities. Furthermore, K||Cu cells were also assessed using Aurbach's method, in which K at a fixed capacity was first deposited on copper foil and then completely stripped, allowing the copper foil to be fully passivated. Thus, K was deposited on copper at 0.5 mAh cm^{-2}, and the K at a specific current density was then stripped and deposited over 10 cycles.

3. Results and discussion

3.1. Manipulation of the ion-association properties of electrolytes

Interactions among various electrolyte components have been considered as an effective principle for electrolyte design, especially for the manipulation of the ion-association properties, transport behavior of cations along with desolvation processes. Moreover, the molecular structures of solvents have also played important roles in electrochemical K-storage reversibility.[22] In this work, electrolytes of bis(fluorosulfonyl)imide potassium salt (KFSI) in mixed solvents of ethylene carbonate (EC) and dimethyl carbonate (DMC) (1 : 1, vol/vol) with different degrees of ion-association were prepared *via* controlling the salt concentrations to increase the ion transport rate (Fig. S1†). Three electrolytes with salt concentration of 1 M, 3 M, and 5 M were prepared, corresponding to low ion-association electrolyte (LIAE), medium ion-association electrolyte (MIAE), and high ion-association electrolyte (HIAE), respectively. Fourier transform infrared (FT-IR) spectroscopy and ultraviolet-visible (UV-vis) spectroscopy were carried out to clarify the change tendency of interactions among electrolyte components with different ion-association properties. The FT-IR spectra shown in Fig. 1a revealed that introducing KFSI into the mixed ester solvents resulted in the appearance of three new shoulder peaks at 1106, 1217, and 1775 cm^{-1}, which were attributable to the interactions between K^+ and electron-rich oxygen atoms in the solvent molecules, with further enhancement of the interaction occurring as the ratio of cations was increased. It is worth observing that the original peaks of the solvents were located at 1069, 1155, 1270, 1748, and 1805 cm^{-1} whereas the position of these peaks was shifted significantly after introducing K^+, evidencing a distinct change in solvation structure. Furthermore, the energy variations calculated from the C–O displacements at 1270 cm^{-1},[28] clearly reveal that significant energy changes (a two-fold increase) were observed when a medium ion-association status in the electrolyte was achieved, thus reflecting a large amount of free solvents being transformed into solvated states (Fig. 1b). This energy change is calculated from eqn (1). A larger energy change means a smaller proportion of free solvent. Further increases in the ion-association demonstrated negligible energy shifts, suggesting the interaction between K^+ and ester solvents has been stabilized. The UV-vis spectra of electrolytes also show a variation in the response of maximum absorption wavelengths owing to the gradual transformation of free solvents into solvated states in the solvation sheath, consistent with the variation in FT-IR signals (Fig. 1c):

$$\Delta E = \frac{hc\Delta v}{1000} \quad (1)$$

Raman spectra, along with the fitted curves, were utilized to further analyze the states of components in electrolytes to demonstrate the differences in ion-association properties of these designed electrolytes.[29] First, the stretching vibrations of S–N–S in the range of 660–780 cm^{-1} were investigated for detecting the interaction of FSI^- with K^+. As shown in Fig. 1d and e, the peak for free EC is located at 717 cm^{-1}, while signals for the solvent-separated ion pairs (SSIP, K^+ without interaction with FSI^-), contact ion-pairs (CIP, K^+ interacting with one FSI^-) and ion aggregates (AGGs, K^+ acting with more than one FSI^-) are positioned at 720, 731 and 741 cm^{-1},

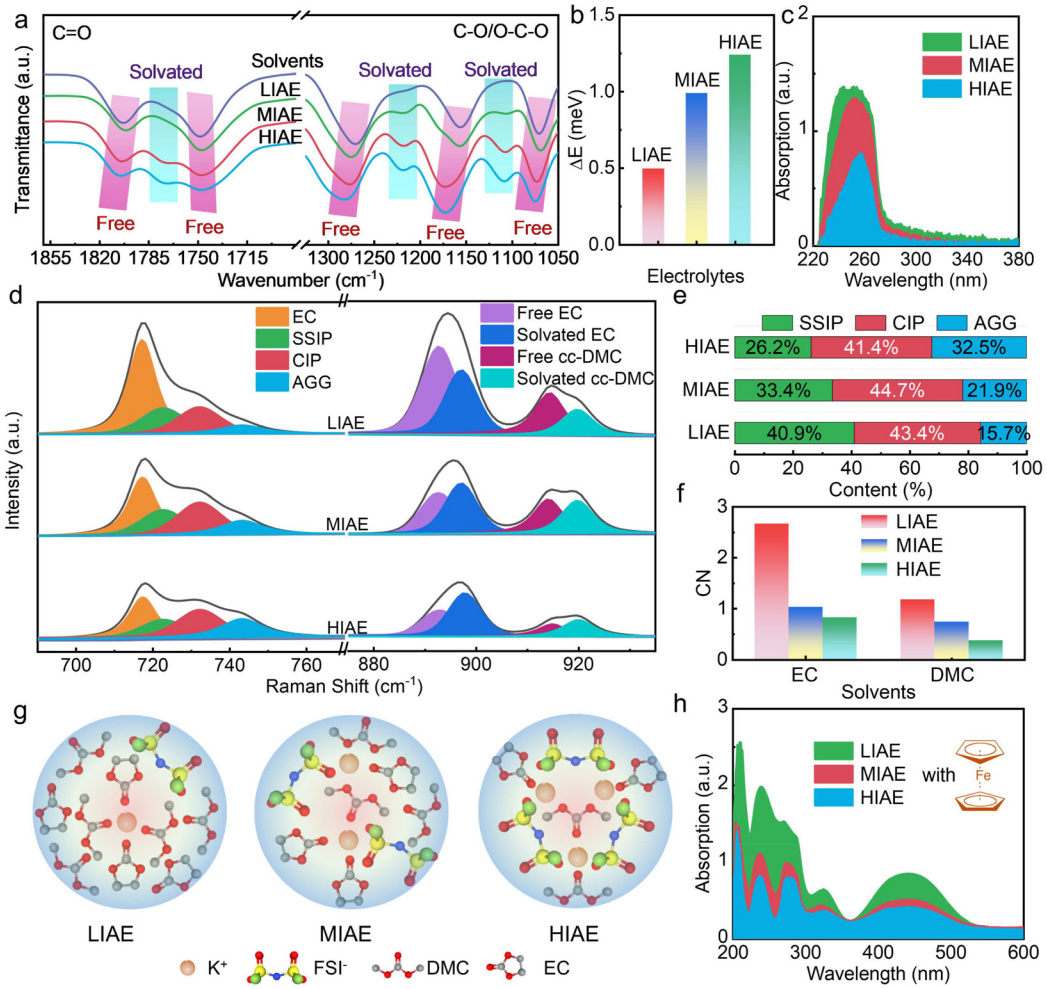

Fig. 1 Manipulation of the ion-association properties of electrolytes: (a) FT-IR spectra; (b) energy values calculated from the peak shifts observed in (a); (c) UV-vis spectra; (d–f) Raman spectra alongside data fitting to obtain ratios for solvation structures and CN; (g) schematic illustrations of K-solvated structures; (h) UV-vis spectral curves of organic material dissolved in electrolytes.

respectively. The solvation structure is mainly composed of SSIP (40.9%) and CIP (43.3%) in the LIAE, with strong interactions between the solvents and K^+. As the proportion of K^+ increased, the content of SSIP in the MIAE further decreased (33.1%) while the contents of CIP and AGGs increased to 44.6% and 22.3%, respectively.

These results supported the enhancement of ion-association between FSI^- and K^+, attributed to the formation of anion-rich solvation structures with significantly suppressed free solvent. Notably, the proportion of FSI^- entering the solvation structure in HIAE is slowed down with increasing cation content, agreeing with the results of FT-IR and UV-vis, as well as further emphasizing the role of cation content in regulating the strength of ion-association in electrolytes.

Four different peaks in the range of 880–930 cm^{-1} are observed at 892.7, 897.3, 914.4, and 920.4 cm^{-1}, corresponding to free EC, solvated EC, free *cis–cis* (cc)-DMC, and solvated cc-DMC, respectively. The high levels of free EC and free DMC in LIAE were responsible for the substantial dissolution of Fc, causing degradation of cycle life (Fig. S2a†). After further elevation of salt concentrations to 3 M, the free solvent percentages are observed to be significantly lowered in MIAE. Specifically, free EC is decreased more significantly than free DMC owing to the stronger solvation effect of EC molecules than DMC. Large amounts of free solvents participate in forming the solvation structure, such that side reactions of free solvent decomposition will be suppressed at low voltage, thus favoring the improvement of interfacial compatibility between the electrolyte and anodes.

In addition, the amount of free solvent has been reduced to 37.8% in HIAE, as evidenced by the shift in peak position and change in area, but this probably decreased the ion transport properties along with increasing the electrolyte viscosity and volume of the solvation structure. Furthermore, the coordination number (CN) values with K^+ from solvents were calculated from the Raman fitting results to gain insight into the evolving solvation structure as a function of ion-association level (Fig. 1f). The observed reduction in CN of EC and DMC

with increasing ion-association proves the progressive displacement of solvent molecules by FSI^- anions within the K^+ solvation shell, forming an anion-rich solvation environment. Conceptual solvation models as shown in Fig. 1g illustrate this transition, visualizing the gradual increase of the salt anion proportion in the solvation structure, which is conducive to enhanced interfacial compatibility. Compared with LIAE and HIAE, MIAE offers a unique balance: it minimizes the presence of free solvents to suppress undesirable side reactions, and exhibits solvent conformation switching for enhancing the solvation ability through the change of salt concentration, thus facilitating the generation of CIP-solvated conformations and ensuring fast reaction kinetics.

The solubility of organometallic compounds in organic electrolytes is dependent on interactions among electrolyte components, resulting in various levels of cycling stability. Therefore, it is essential to explore the active substance solubility in designed electrolytes to ensure proper operation of the cell. An experiment to investigate the solubility of trace amounts for Fc was conducted in three electrolytes, as shown in Fig. S2b.† The result demonstrated that the solubility problem was significantly suppressed with the enhancement of ion-association. Furthermore, the phenomenon of hierarchical layering appeared in MIAE, offering a prerequisite for realizing high-capacity and long-term performances.[30] Moreover, UV-vis spectra were recorded in clear solutions selected from the solubility tests with the spectrum of the corresponding electrolyte as the background. Fig. 1h visually shows a notable weakening of the response peak to Fc in MIAE and a further decrease in HIAE. This proves that modification by tuning ion-association properties can significantly resolve the problem and reduce the occurrence of side reactions. Electrolytes are closely related to the safety of batteries in addition to their tasks of improving electrochemical performance. Thus, the flame-retardant properties of the three different electrolytes were tested to demonstrate their usefulness. As shown in Fig. S2c,† the maximum flame height of the electrolyte is selected as a reference during the combustion test, revealing that a gradual increase in K^+ content will result in a progressive lowering of combustion intensity. This behavior is attributed to the effects of solvation structure modulation on the electrolyte allowing large amounts of free solvent to participate in the configuration of CIP and AGGs to enable enhancement of flame retardancy.

Electrolyte strategy and battery performance depend greatly on the viscosity of the working electrolyte. Viscosity affects the ion diffusion rate, conductivity, and wettability of the electrolyte. Wettability experiments were conducted on LIAE, MIAE and HIAE and the results are shown in Fig. S3,† where the viscosity of HIAE is much larger than that of LIAE and MIAE. Subsequently, conductivity and K^+ transference number were tested for LIAE, MIAE and HIAE. The results of the conductivity tests coincided with the results of the contact angle, and MIAE had the highest K^+ transference number ($t_{K^+} = 0.58$) (Fig. S4†).

In order to verify the effect of ionic binding on K plating/stripping behavior, K||Cu asymmetric and K||K symmetric cells were studied. As shown in Fig. S5a–d,† MIAE with a current density of 0.25 mA cm^{-2} and a fixed capacity of 0.25 mAh cm^{-2} exhibits the highest and most stable coulombic efficiency in the K||Cu cell, indicating that K deposition and stripping in MIAE is highly reversible and side reactions are effectively suppressed. MIAE has the lowest polarization voltage in the K||K symmetric cell and exhibits excellent K reversible plating/stripping, suggesting that MIAE is able to maintain long-term cycling stability (Fig. S5†).

3.2. K-storage performance of Fc in different ion-association electrolytes

To explore the compatibility of Fc electrodes in different ion-association electrolytes as well as the K-storage behaviors, coin cells were assembled to test electrochemical properties with K as the counter electrode. The cycling performance of Fc in the design electrolytes at a current density of 50 mA g^{-1} is shown in Fig. 2a. The reversible capacity of the Fc anode in LIAE exhibited a tendency of gradual decay with cycling; the discharge capacity was 161.8 mAh g^{-1} after 200 cycles, which may be attributed to the decomposition of free solvents on electrode surfaces together with a small amount of dissolved active substances. Fc exhibited the best electrochemical performance in MIAE with a capacity of up to 210.9 mAh g^{-1} after 200 cycles and an average CE of more than 99.5%, being associated with a change in the solvation configuration of electrolytes that reduces the proportion of free solvent as well as enhances the strength of ion-association. However, the capacity of Fc in HIAE was decreased with increasing salt concentration, owing to the increase in electrolyte viscosity and solvation structure volume. Table S1† shows the significant improvement in K-storage performance of ferrocene in MIAE compared to different organic anodes.

The galvanostatic discharge/charge curves (GDC) for the Fc anode in the designed electrolytes subjected to different cycling are shown in Fig. 2b and Fig. S6a–c.† The presented curves had no obvious intercalation/deintercalation K plateau, and demonstrated that the active substance is stored by an adsorption/desorption storage mechanism for K. The charge/discharge curves of Fc in MIAE exhibited a high degree of reversibility and cycling stability, while the capacity and cycle life in the other two electrolytes revealed a trend of decay, reflecting the fact that matching electrolytes can increase the electrochemical performance of Fc materials. Differential capacity curves (dQ/dV) at the 50^{th} cycle were applied to verify the redox potential changes for Fc during the K-storage process in electrolytes with different ion-association levels, as shown in Fig. 2c. In MIAE and HIAE, there was no obvious reaction plateau for Fc with a weak pair of oxidation and reduction peaks at 0.87 and 0.22 V, whereas the reaction potential in LIAE was significantly shifted, demonstrating an unstable K-storage reaction.

The calculation of the average potential in GDC curves after cycling stabilization can reflect the difference in polarization due to the internal impedance of cells during the process, a key indicator of the reaction kinetics. In Fig. S6d,† the average

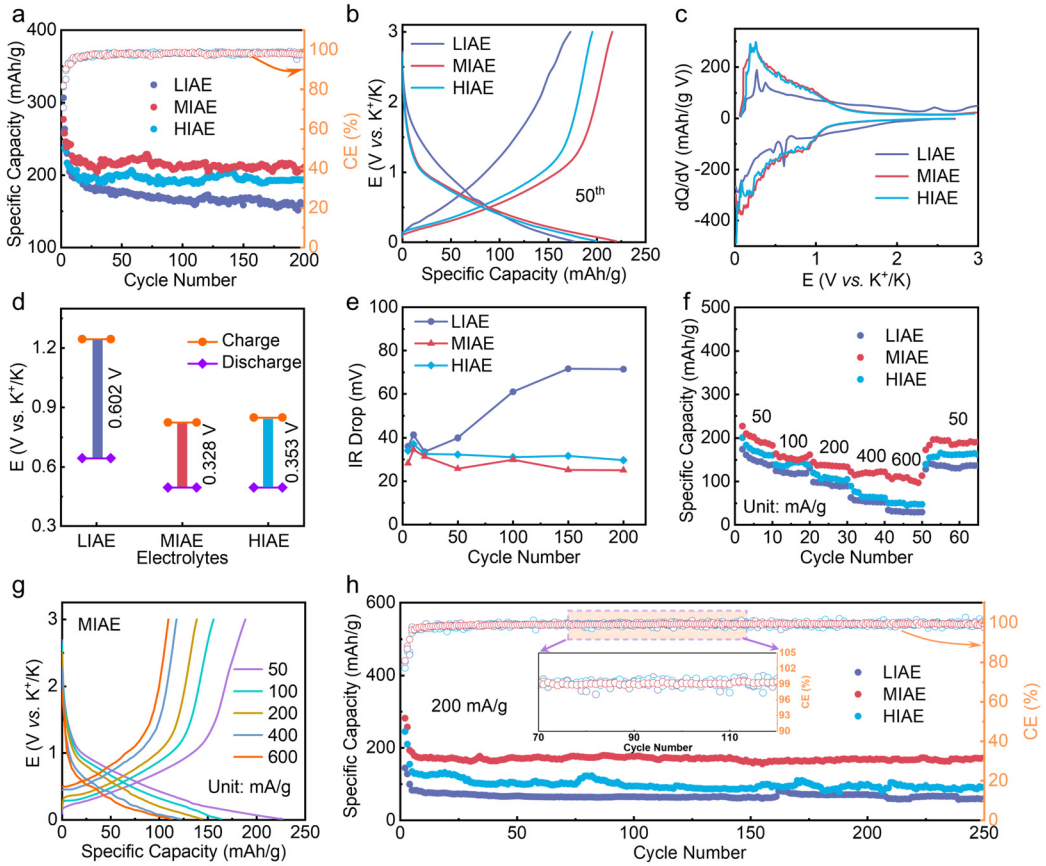

Fig. 2 K-storage performance of Fc in different ion-association electrolytes: (a) cycling performance at 50 mA g^{-1}; (b) GDC curves at the 50th cycle and (c) its corresponding dQ/dV curves; (d) average K-storage potentials; (e) IR drop values over different cycles; (f) rate performance; (g) GDC curves at various rates in the MIAE; (h) cycling performance at 200 mA g^{-1} (inset: local enlargement).

potential is obtained by integrating the area of closed intervals formed by the capacity and the points of intersection with the coordinate axes. Specifically, the average potential is 0.328 V in the MIAE, with a minimal difference between charge and discharge relative to the other two electrolytes (Fig. 2d). To further validate our speculation, the change in impedance during cycling was calculated by IR-drop as shown in Fig. S7a.† A minimum IR-drop was always maintained in the MIAE with the fastest reaction kinetics regardless of the number of cycles as compared to other electrolytes (Fig. 2e).

The Fc anode can exhibit excellent rate performance at higher current densities, which is attributed to faster electron transfer rates and excellent reaction kinetics. In the MIAE, it proved to be highly reversible as Fc showed discharge specific capacities of 209, 165, 140, 129, and 114 mAh g^{-1} at current densities of 50, 100, 200, 400, and 600 mA g^{-1}, respectively, and could still provide a specific capacity of 200 mAh g^{-1} when the current density was restored to 50 mA g^{-1}. In contrast, the Fc anode could only provide discharge specific capacities of 155, 126, 101, 57, and 35 mAh g^{-1} in LIAE, and 184, 149, 115, 70, and 52 mAh g^{-1} in HIAE at the same current densities, and an inferior rate capability performance (Fig. 2f). Besides, the GDC curves of Fc at different current densities in MIAE have similar shapes as well as relatively small variations of polarization, and this behavior is directly related to the solvation structure of anion-rich electrolytes and medium ion-association intensity, as shown in Fig. 2g and Fig. S7b, c.†

The excellent cycling stability of Fc observed at large current density is also noted thanks to the regulation of the degree of ion-association. The electrochemical performance of the design electrolytes is recorded in Fig. 2h and Fig. S8† at 200 mA g^{-1}, and demonstrates a high reversible capacity of 171.9 mAh g^{-1} after 250 cycles in MIAE with stability during cycling and an average CE as high as 99.8%. In comparison, the Fc anode shows lower reversible capacity (60.2 mAh g^{-1}) in LIAE, which is associated with lower carrier numbers as well as weaker ion-association intensity. Nevertheless, the discharge capacity of Fc in HIAE significantly decayed relative to the capacity at 50 mA g^{-1} after the viscosity of the electrolyte increased and the ion-transport speed slowed.

3.3. K-storage kinetics of Fc in different ion-association electrolytes

To verify the effect of modulating ion-association strength on the reaction kinetics and ion-transport properties of Fc anode

materials, an in-depth analysis was carried out using the galvanostatic intermittent titration technique (GITT) and *in situ* electrochemical impedance spectroscopy (EIS) measurement. The GITT curves obtained for the Fc anode in different ion-association electrolytes at a current density of 50 mA g^{-1} and certain cutoff voltages of 0.01–3.0 V are shown in Fig. 3a, where the interval time is 20 min followed by a resting time of 1 h. It can be visualized that the capacity of Fc in MIAE is higher than that in the other two electrolytes, which is inevitably related to the transport of K^+ in the electrolyte and rapid reaction kinetics. The resting phase of the charging/discharging process in the GITT test leads to variation in potential as a result of self-discharge of cells, called overpotential (η), a value that is smaller, proving superior kinetic properties. In Fig. 3b, the calculated η for the Fc anode in MIAE is significantly lower compared to that in other electrolytes, implying this electrolyte and the electrode material system have the lowest impedance value.

$$D_{K^+} = \frac{4}{\pi\tau}\left(\frac{n_m V_m}{S}\right)^2\left(\frac{\Delta E_s}{\Delta E_t}\right)^2 = \frac{4L^2}{\pi\tau}\left(\frac{\Delta E_s}{\Delta E_t}\right)^2 \quad (2)$$

In addition, the diffusion coefficient of K^+ can be calculated by Fick's second law eqn (2),[31] where L is the thickness of the anode slurry coating, τ is the resting time, ΔE_s is the potential difference caused by a period of pulsed current, and ΔE_t is the potential difference resulting from one cycle of the work section. The tendency of the D_{K^+} value to decrease with decreasing potential during the process of potassiation, as shown in Fig. 3c and Fig. S9,† is due to the K-storage chemical reaction that occurs at low potentials being determined by the speed of the charge transfer. However, the values of D_{K^+} under electrolytes with different

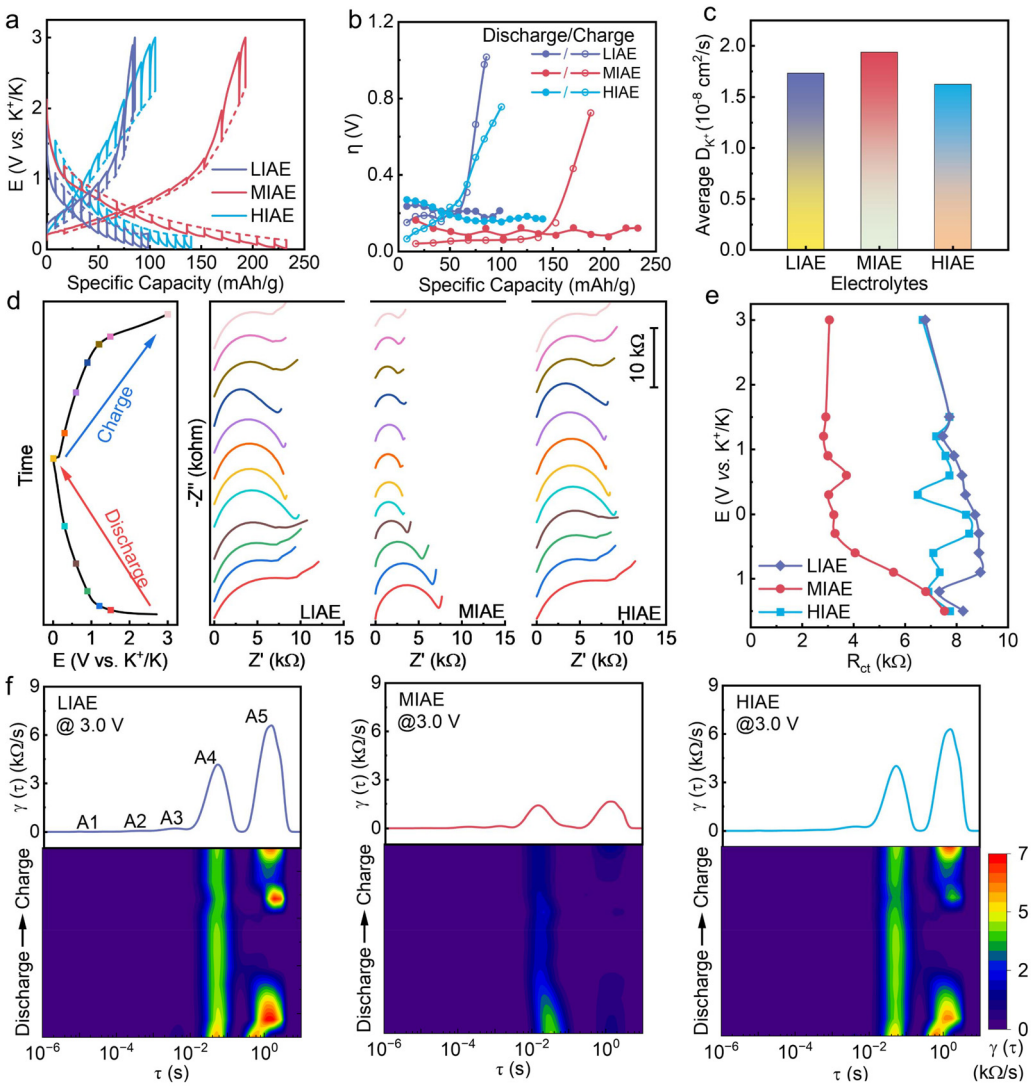

Fig. 3 K-storage kinetics of Fc in different ion-association electrolytes: (a) GITT curves, (b) corresponding overpotential (η) and (c) average D_{K^+} values; (d) *in situ* EIS spectroscopy and (e) evolution of R_{ct} in the electrolytes; (f) DRT results of LIAE, MIAE and HIAE for *in situ* EIS plots.

ion-association properties vary at the same potential. Among them, Fc was found to exhibit the largest D_{K^+} value in MIAE attributed to the anion-rich solvation structure with medium ion-association, thus demonstrating the excellent transport and reaction kinetics of this K-storage system. However, the viscosity of the HIAE becomes larger, and the ion-transport rate slows down, so the D_{K^+} value is smaller than that of LIAE and MIAE.

In situ EIS was performed to examine the evolution of Fc anode interfaces with various electrolytes, which can be demonstrated by ion-diffusion impedance, charge-transfer impedance (R_{ct}) and ohmic contact resistance (R_e) (Fig. 3d). The high-frequency wavelength of the Nyquist curve for cells is represented as R_{ct}, the trend of which can allow the fast or slow charge-transfer kinetics as a prerequisite for excellent electrochemical performance to be visualized. The R_{ct} of Fc in electrolytes with different ion-association properties are shown in Fig. 3e, obtained according to the equivalent circuit fitting shown in Fig. S10.† With respect to the Fc||LIAE system, R_{ct} gradually increases throughout the discharge process, which is related to the decomposition of ester-based solvents to form the organic-dominated SEI layer. However, the discharge process of Fc demonstrates an increasing and then decreasing trend of R_{ct} caused by the formation of the SEI film in MIAE, and R_{ct} is then finally stabilized, which indicates that the stability of the Fc anode structure has been better protected. The same trend can be observed in HIAE, but Fc is unable to achieve enhanced rate performance and cycling under high currents in a high-viscosity system.

In addition, as shown in Fig. 3f, the distribution of relaxation time (DRT) curves acquired by *in situ* EIS spectroscopy for the Fc anode was collated to further explain the differences in the formation of the SEI among the three electrolytes with different solvation structures. The five different peaks (A1–A5) recorded correspond to different processes: A1–A3 ($\sim 10^{-3}$ s) originate from the electric and magnetic fields generated by particle–particle and particle–collector interactions; A4 ($\sim 10^{-2}$ s) corresponds to ion transport (R_{SEI}); and A5 ($\sim 10^{0}$ s) corresponds to the charge-transfer process in Fc (R_{ct}).[32] Compared to the other two electrolyte systems, the R_e, R_{SEI} and R_{ct} values for the Fc anode are lower and more stable during charging and discharging in the MIAE system, which can be attributed to the fact that the anion-rich solvation structure with medium ion-association degree facilitates fast reaction kinetics and enables fast and stable K-storage.

3.4. Electrolyte solvent-dependent K-storage properties and mechanism

Effects on ion-association of electrolytes and electrochemical properties of the Fc active substance with respect to salt content were explored as described above without discussing the effect of structural changes of solvent molecules. Hence, 3 M KFSI/PC + DMC (PC-based MIAE) and 3 M KFSI/VC + DMC (VC-based MIAE) electrolytes were designed to investigate the difference in electrochemical performance of Fc from that in EC-based MIAE, with the aim of explaining more in-depth the influence of the electrolyte's physicochemical properties on the stability of electrode structure as well as the electrochemical properties of K-storage. The reversible capacity of Fc in the VC-based MIAE, as shown in Fig. 4a, demonstrates a rapidly decaying tendency during cycling at 100 mA g^{-1}; a discharge capacity of only 36.1 mAh g^{-1} is retained after 10 cycles, and the capacity retention is merely 7.9%, which is caused by the structural instability of VC, which is prone to form oligomers and significantly suppresses K^+ transport.[33] In the PC-based MIAE, the Fc anode also revealed capacity decay during the first 50 cycles accompanied by fluctuations in CE, due to the addition of branched chains to the molecular structure.[34] However, Fc retained its highest capacity in the EC-based MIAE; after 200 cycles, the reversible capacity is maintained at 206.8 mAh g^{-1} with an average CE of more than 99%. The GDC curves of Fc at the 100th cycle indicated the lowest polarization occurred in the EC-based MIAE with no significant change during cycling, as shown by stable cycling curves (Fig. 4b and Fig. S11a–c†). In contrast, polarization in the other two electrolytes is greater and tends to increase with cycling. The higher discharge capacity and faster kinetic properties of Fc in the EC-based MIAE demonstrate the dependence on electrolyte design. Since the VC-based MIAE is poorly compatible with the Fc anode, the K-storage performance in the other two electrolytes is discussed subsequently and the charge storage mechanism is explored in depth.

It is observed that the rate performance of Fc in the EC-based MIAE as shown in Fig. 4c and Fig. S11d† is superior to that in the PC-based MIAE with faster redox reaction kinetics. Besides, the IR-drop curves of Fc corresponding to various cycles in both electrolytes are shown in Fig. 4d and Fig. S11e, f,† and these consistently maintain minimum IR-drop values in the EC-based MIAE. Therefore, the EIS before and after analysis using cyclic voltammetry (CV) further explains the above situation, with the spectra exhibited after equivalent circuit fitting of the Nyquist plots, where R_{ct} shows a trend of decreasing impedance after cycling in both electrolytes to reflect the generation of relatively stable interfacial layers. In particular, R_{ct} decreased from 7.3 kΩ to 2.5 kΩ in the EC-based MIAE while R_{ct} decreased from 12.1 kΩ to 3.8 kΩ in the PC-based MIAE, confirming that Fc possesses a faster charge-transfer rate in the EC-based MIAE (Fig. 4e).

A systematic investigation of the charge-storage mechanisms of Fc in different electrolytes has also been carried out using the CV test technique. As shown in Fig. 4f and Fig. S12,† the shapes of the CV curves for Fc in different electrolytes are highly similar, and the intensity of the response peaks gradually increase with increasing scan rate. There is no obvious change in the peak shape of response peaks in the EC-based MIAE, which demonstrates stable K-storage performance, but the peak shape collapses with increasing scan rate in the PC-based MIAE, reflecting that the electrode material and the electrolyte have poor compatibility.

$$i = av^b \tag{3}$$

$$\ln i = \ln a + b \ln v \tag{4}$$

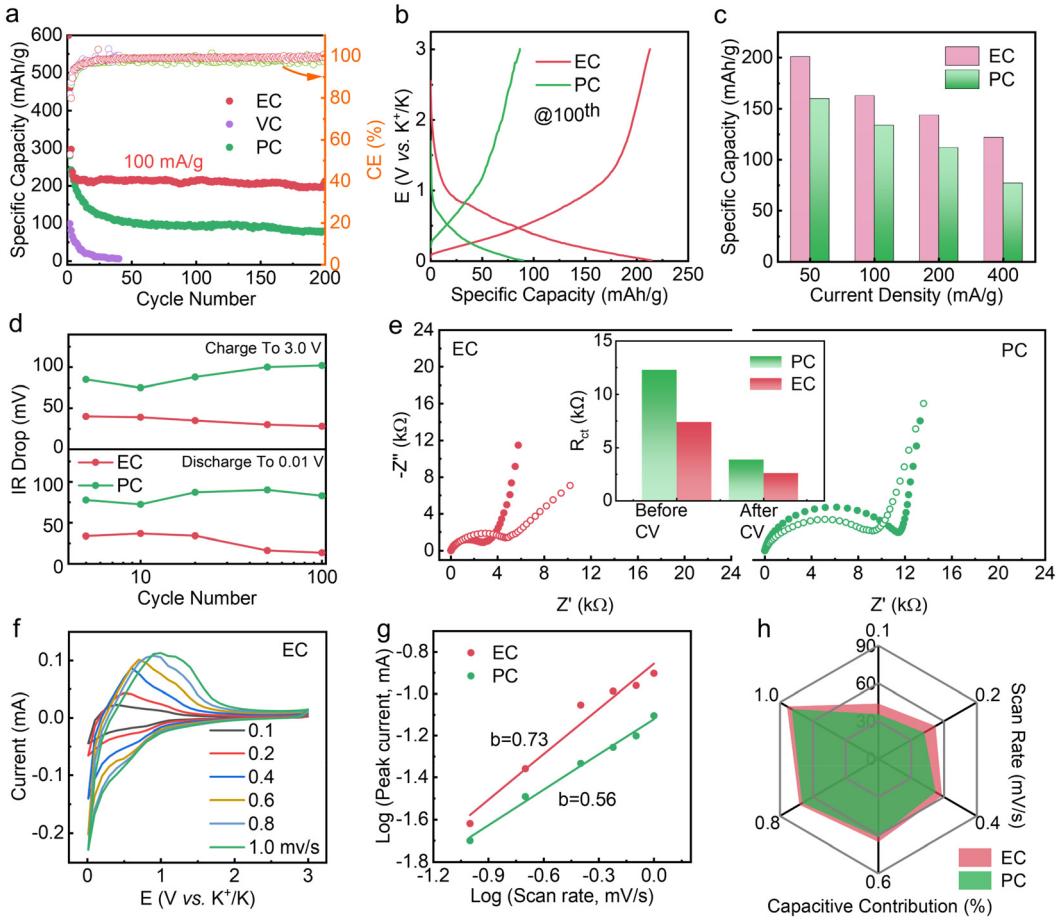

Fig. 4 Electrolyte solvent-dependent K-storage properties and mechanism: (a) cycling performance at 100 mA g^{-1} and (b) GDC curves at the 100th cycle; (c) rate performance; (d) IR drop for EC-based and PC-based MIAEs; (e) EIS curves, (inset: evolution of R_{ct} before and after CV); (f) CV curves of Fc in the EC-based MIAE; (g) as-calculated *b* values for anodic peaks; (h) comparison of capacitance contributions to the K-storage mechanism.

$$i = k_1 v + k_2 v^{1/2} \quad (5)$$

$$i/v^{1/2} = k_1 v^{1/2} + k_2 \quad (6)$$

The relationship between peak current (i) and corresponding scan rate (v), according to the CV curves shown in Fig. 4g,[35,36] follows eqn (3) and (4) where the coefficients a and b are constants that can be used to quantitatively analyze the charge-storage mechanism. Therein, the semi-infinite linear diffusion-controlled process is denoted by the b value that is infinitely near to 0.5, while the capacitance-controlled process is the b value that is infinitely near to 1.0. The CV curves are calculated by fitting the b values of 0.73 and 0.56 for Fc in the EC-based and PC-based MIAEs, respectively. This trend suggests that the shift from diffusion-dominated storage mechanisms to pseudocapacitance-controlled ones is favored for Fc in the EC-based MIAE. In addition, the proportions of pseudocapacitive and diffusive behaviors were further calculated using eqn (5) and (6).[37,38] Specifically, the percentage of the pseudocapacitance contribution of the Fc anode is relatively low at low scan rates in both electrolytes, but its pseudocapacitance contribution gradually increases with increasing scan rate, which clearly demonstrates the transition of the charge-storage mechanism. The pseudocapacitance-controlled process in the EC-based MIAE accounts for a somewhat larger proportion, enhancing the reaction kinetics in this regime (Fig. 4h and Fig. S13, S14†).

X-ray photoelectron spectroscopy (XPS) was used to analyze the differences in the SEI layers produced by the EC-based MIAE and the PC-based MIAE on the Fc surface. The SEI formed by the EC-based MIAE has a higher ratio of O, F and K, indicating that the EC-based MIAE forms more interfacial phases consisting of inorganic components on the Fc surface (Fig. S15a†). The high-resolution XPS spectra of F 1s and K 2p are shown in Fig. S15b and c.† Two fluorine-related species, attributed to the K–F species (683.3 eV) and the S–F species (687.8 eV), are present in the F 1s spectrum. The presence of the K–F species indicates that the S–F bonds are cleaved during SEI formation, and a K–F-rich SEI layer is effective in inhibiting dendrite formation and contributing to stability. The K–F-rich SEI layer can effectively inhibit the formation of metal dendrites and contributes to the stability. High-resolu-

tion K 2p spectroscopy shows that the SEI formed by Fc in both electrolytes contains K–O (293.2, 295.9 eV) and K–F (292.7, 295.5 eV) bonds. The presence of prominent K–F signals derived from the SEI layers formed by the EC-based MIAE suggests that anion-dominated solvation can be achieved by a solvent design strategy.

3.5. Compatibility testing for the optimized EC-based MIAE system

To verify that the optimized solvation structure formed by the electrolyte is conducive to achieving excellent K plating/stripping behavior, in-depth investigations were carried out to investigate the cycle life, overpotential variation, and CE stability of K||Cu asymmetric and K||K symmetric cells. As illustrated in Fig. S16a, b and c,† the EC-based MIAE at a current density of 0.1 mA cm^{-2} and fixed capacity of 0.1 mAh cm^{-2} demonstrates higher CE and lower voltage polarization than the PC-based MIAE in K||Cu cells, proving favorable compatibility with K metal.

The rate performance of K||Cu cells in both electrolytes was also tested, with decreased polarization and excellent kinetics in the EC-based MIAE at current densities of 0.1, 0.2, 0.4, 0.6, 0.8, and 1 mA cm^{-2} and at specific capacity of 1 mAh cm^{-2} (Fig. S17a†). Furthermore, a larger polarization and a lower CE value in rate performance tests in the PC-based MIAE under the abovementioned conditions, as shown in Fig. S17b,† indicate the occurrence of substantial numbers of side reactions. Specifically, the K||Cu cell in the EC-based MIAE delivers potential polarization of 0.08, 0.13, 0.21, 0.24, 0.27, and 0.28 V at the above current densities, respectively, with this value not dramatically changing by increasing current densities, which is attributed to the formation of stable interfacial layers (Fig. 5a). Using the Aurbach method, the CE of two design electrolytes was explored, calculated by dividing the total stripping capacity by its total plating capacity, and pre-cycling of Cu for passivation prior to this procedure was required. The K||Cu cell in the EC-based MIAE was revealed to provide up to 91.93% CE, which is higher than that of the PC-based MIAE. This result reflects both the enhanced reversibility of K plating/stripping and the excellent electrolyte–electrode compatibility (Fig. 5b).

The K||K symmetric cells were prepared with both the EC-based and PC-based MIAE, as shown in Fig. 5c, to further validate their long-term cycling performance. Therein, the voltage hysteresis in the PC-based MIAE was 0.44 V, and after 500 h of cycling, K exhibited asymmetric deposition/dissolution behavior, probably attributable to the generation of large amounts of "dead K". In contrast, the K||K cell in the EC-based MIAE exhibited an average voltage hysteresis of around 0.16 V as well as stable cycling for 800 h without significant changes in

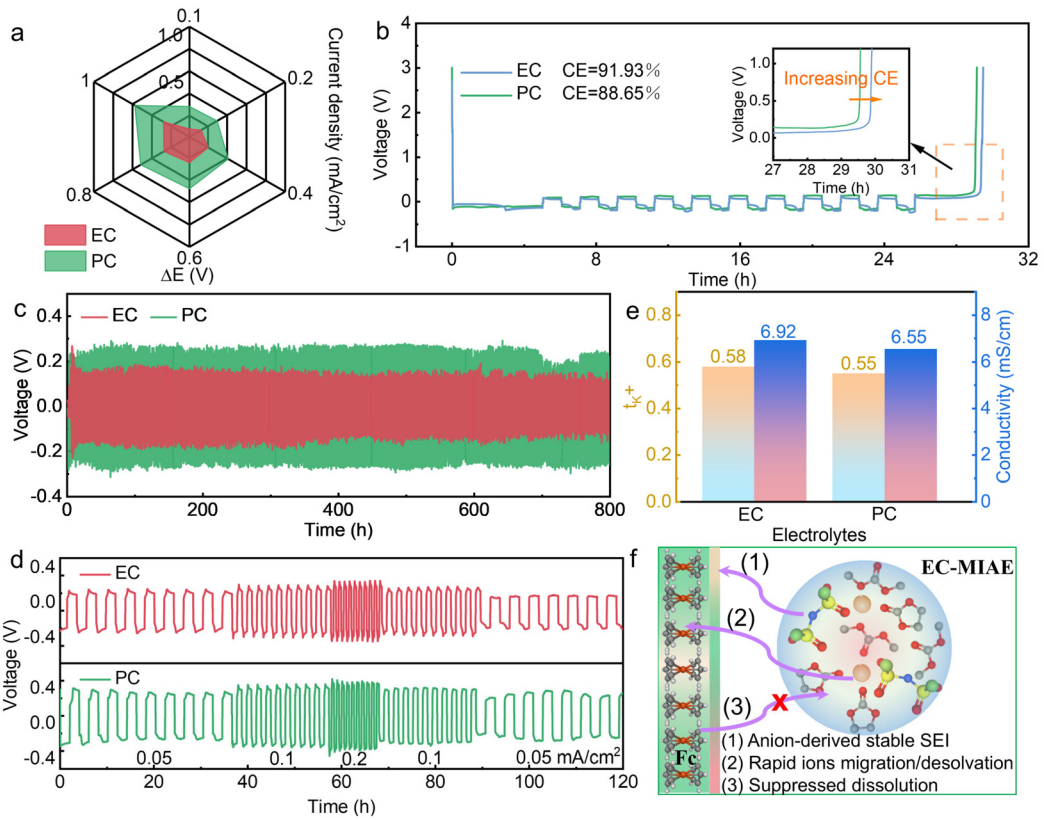

Fig. 5 Compatibility testing for the optimized EC-based MIAE system: (a) potential polarization for voltage profiles of the K||Cu cell with the EC-based MIAE at different current densities; (b) CE of K||Cu cells through Aurbach's test; (c) cycling performance and (d) rate performance of K||K symmetric cells; (e) ionic conductivity and transference number; (f) working principle of the EC-based MIAE.

voltage hysteresis, which is a result of the modulation of ion-association properties enhancing the compatibility of the electrolyte with K. In addition, the rate performance of K||K symmetric cells with both electrolytes was also tested, as the current density was increased from 0.05 to 0.2 and then decreased to 0.05 mAh cm^{-2}. It was found that a relatively low voltage hysteresis was consistently maintained throughout the tests with the EC-based MIAE compared to that with the PC-based MIAE with no sharp changes in voltage (Fig. 5d). The samples could then still sustain normal cycling when the current density was returned to low current values.

In order to further validate the excellent transport kinetics in the EC-based MIAE, its ion mobility number (t_{K^+}) as well as conductivity were tested. With the constant potential polarization method, as shown in Fig. 5e and Fig. S18,† the t_{K^+} in EC-based and PC-based MIAEs were found to be 0.58 and 0.55, respectively. It is demonstrated that the EC with lower viscosity possesses higher mobility compared to the PC, which reduces the concentration polarization during charging and discharging to improve the kinetic performance of cells. Conductivity is generally dependent on two factors, K^+ concentration and mobility. The conductivity of the EC-based MIAE (6.92 mS cm^{-1}) will be higher than that of the PC-based MIAE (6.55 mS cm^{-1}) when the carriers are at the same level. A comprehensive comparison involving optimized and incompatible electrolytes demonstrated that fast transport kinetics, reduced proportion of free solvent, and high-quality interfacial layers are crucial for the excellent electrochemical performance and stable cycle life of Fc anodes, thus enabling enhanced performance (Fig. 5f).

4. Conclusion

In summary, a green and environmentally friendly MIAE was developed for Fc-based organic K-storage anodes. The MIAE exhibited high ionic conductivity, anion-rich solvation structures, as well as a significant reduction of free solvent content, thereby addressing critical challenges such as dissolution of active materials, poor interfacial stability, and sluggish reaction kinetics during the K-storage process. As a result, the Fc anode in the MIAE can deliver a high reversible specific capacity of 209.1 mAh g^{-1} after 200 cycles at 50 mA g^{-1} with an average CE of above 99.7%. This work presents an electrolyte engineering strategy for balancing thermodynamic and kinetic requirements and thus realizing fast and stable K-storage devices.

Author contributions

Jing Zheng: writing – review & editing, investigation, funding acquisition, conceptualization. Qun Li: writing – original draft, investigation, formal analysis, data curation. Hao Wang: methodology, investigation, formal analysis. Jijian Xu: funding acquisition, methodology, validation, writing – review & editing. Xiaokang Chu: investigation, validation, formal analysis. Ran Chen: validation, methodology, investigation. Haobo Xia: formal analysis, conceptualization. Jianying Long: validation, methodology, investigation. Meng Lei: visualization, validation. Mengtao Ma: writing – review & editing, resources. Zixia Lin: visualization, validation. Qingxue Lai: writing – review & editing, supervision, funding acquisition.

Conflicts of interest

The authors declare no competing financial interest.

Data availability

All data included in this study are available upon request by contact with the corresponding authors.

Acknowledgements

We gratefully acknowledge support from the National Natural Science Foundation of China (Grant No. 52402312, 22005148 and 21902077), the Natural Science Foundation of Jiangsu Province (Grant No. BK20200766 and BK20190381), the Research Grants Council of Hong Kong (Grant No. C1002-24Y), the Environment and Conservation Fund (ECF Project 20/2023), and the Science Technology and Innovation Committee of Shenzhen Municipality (JCYJ20240813153120027).

References

1 Y. Tian, G. Zeng, A. Rutt, T. Shi, H. Kim, J. Wang, J. Koettgen, Y. Sun, B. Ouyang, T. Chen, Z. Lun, Z. Rong, K. Persson and G. Ceder, *Chem. Rev.*, 2021, **121**, 1623–1669.
2 S. Li, J. Huang, Y. Cui, S. Liu, Z. Chen, W. Huang, C. Li, R. Liu, R. Fu and D. Wu, *Nat. Nanotechnol.*, 2022, **17**, 613–621.
3 L. Tu, Z. Zhang, Z. Zhao, X. Xiang, B. Deng, D. Liu, D. Qu, H. Tang, J. Li and J. Liu, *Angew. Chem., Int. Ed.*, 2023, **62**, e202306325.
4 R. Schmuch, R. Wagner, G. Hörpel, T. Placke and M. Winter, *Nat. Energy*, 2018, **3**, 267–278.
5 Y. Chu, J. Zhang, Y. Zhang, Q. Li, Y. Jia, X. Dong, J. Xiao, Y. Tao and Q. Yang, *Adv. Mater.*, 2023, **35**, 2212186.
6 X. Chen, M. Xie, Z. Zheng, X. Luo, H. Jin, Y. Chen, G. Yang, D. Bin and D. Li, *J. Am. Chem. Soc.*, 2023, **145**, 5105–5113.
7 K. Qin, K. Holguin, J. Huang, M. Mohammadiroudbari, F. Chen, Z. Yang, G. Xu and C. Luo, *Adv. Sci.*, 2022, **9**, 2106116.
8 Y. Lu and J. Chen, *Nat. Rev. Chem.*, 2020, **4**, 127–142.
9 Y. Xie, H. Lu, J. Huang and H. Xie, *Adv. Funct. Mater.*, 2023, **33**, 2213910.
10 T. Sun, J. Xie, W. Guo, D. Li and Q. Zhang, *Adv. Energy Mater.*, 2020, **10**, 1904199.

11 J. Yan, Y. Cui, M. Xie, G. Yang, D. Bin and D. Li, *Angew. Chem., Int. Ed.*, 2021, **60**, 24467–24472.
12 X.-X. Luo, W. Li, H. Liang, H. Zhang, K. Du, X. Wang, X. Liu, J. Zhang and X. Wu, *Angew. Chem., Int. Ed.*, 2022, **61**, e202117661.
13 Y. Hu, W. Tang, Q. Yu, X. Wang, W. Liu, J. Hu and C. Fan, *Adv. Funct. Mater.*, 2020, **30**, 2000675.
14 Y. Zhao, Y. Ding, J. Song, G. Li, G. Dong, J. B. Goodenough and G. Yu, *Angew. Chem., Int. Ed.*, 2014, **53**, 11036–11040.
15 C. Li, C. Zhang, J. Xie, K. Wang, J. Li and Q. Zhang, *Chem. Eng. J.*, 2021, **404**, 126463.
16 Z. Sun, K. Xi, J. Chen, A. Abdelkader, M. Li, Y. Qin, Y. Lin, Q. Jiang, Y. Su, R. Vasant Kumar and S. Ding, *Nat. Commun.*, 2022, **13**, 3209.
17 S. Zhang, B. Liang, Y. Fan, J. Wang, X. Liang, H. Huang, D. Huang, W. Zhou and J. Guo, *ACS Appl. Mater. Interfaces*, 2019, **11**, 31943–31953.
18 Z. Liu, L. Feng, X. Su, C. Qin, K. Zhao, F. Hu, M. Zhou and Y. Xia, *J. Power Sources*, 2018, **375**, 102–105.
19 S. Zhang, B. Liang, Y. Fan, J. Wang, X. Liang, H. Huang, D. Huang, W. Zhou and J. Guo, *ACS Appl. Mater. Interfaces*, 2019, **11**, 31943–31953.
20 M. Li, C. Wang, Z. Chen, K. Xu and J. Lu, *Chem. Rev.*, 2020, **120**, 6783–6819.
21 J. Wu, Q. Zhang, S. Liu, J. Long, Z. Wu, W. Zhang, W. K. Pang, V. Sencadas, R. Song, W. Song, J. Mao and Z. Guo, *Nano Energy*, 2020, **77**, 105118.
22 L. Fan, H. Xie, Y. Hu, Z. Caixiang, A. M. Rao, J. Zhou and B. Lu, *Energy Environ. Sci.*, 2023, **16**, 305–315.
23 H. Xie, H. Liang, P. Kumar, H. Cheng, F. Zhao, Y. Wang, T. Cai, W. Wahyudi, Z. Ma, Q. Li and J. Ming, *Adv. Funct. Mater.*, 2024, **34**, 2401118.
24 Z. Zha, D. Li, T. Sun, Q. Sun, J. Hou, Z. Tao and J. Chen, *J. Am. Chem. Soc.*, 2024, **146**, 31612–31623.
25 O. Sheng, T. Wang, T. Yang, T. Jin, X. Tao and C. Jin, *Nano Energy*, 2024, **123**, 109406.
26 R. Sun, T. Wang, Q. Fan, M. Wu, X. Yang, X. Wu, Y. Yu, X. Xia, F. Cui, J. Wan, X. Lu, X. Hao, A. K. Y. Jen, E. Spiecker and J. Min, *Joule*, 2023, **7**, 221–237.
27 R. Lin, C. Ke, J. Chen, S. Liu and J. Wang, *Joule*, 2022, **6**, 399–417.
28 D. Prat, A. Wells, J. Hayler, H. Sneddon, C. R. McElroy, S. Abou-Shehada and P. J. Dunn, *Green Chem.*, 2016, **18**, 288–296.
29 H. Tu, L. Li, Z. Wang, J. Wang, H. Lin, M. Wang, C. Yan and M. Liu, *ACS Nano*, 2022, **16**, 16898–16908.
30 Y. Yao, X. Chen, C. Yan, X. Zhang, W. Cai, J. Huang and Q. Zhang, *Angew. Chem., Int. Ed.*, 2021, **60**, 4090–4097.
31 S. Samaroo, C. Hengesbach, C. Bruggeman, N. G. G. Carducci, L. Mtemeri, R. J. Staples, T. Guarr and D. P. Hickey, *Nat. Chem.*, 2023, **15**, 1365–1373.
32 Y. Tang, J. Chen, Z. Mao, C. Roth and D. Wang, *Carbon Energy*, 2023, **5**, e257.
33 J. Zhang, X. Yue, Z. Wu, Y. Chen, Y. Bai, K. Sun, Z. Wang and Z. Liang, *Nano Lett.*, 2023, **23**, 9609–9617.
34 Y. Zhang, Y. Katayama, R. Tatara, L. Giordano, Y. Yu, D. Fraggedakis, J. G. Sun, F. Maglia, R. Jung, M. Z. Bazant and Y. Shao-Horn, *Energy Environ. Sci.*, 2020, **13**, 183–199.
35 Y. Wang, Z. Cao, Z. Ma, G. Liu, H. Cheng, Y. Zou, L. Cavallo, Q. Li and J. Ming, *ACS Energy Lett.*, 2023, **8**, 1477–1484.
36 Z. Huang, M.-T. Yang, J. Qi, P. Zhang, L. Lei, Q. Du, L. Bai, H. Fu, X.-S. Yang, R. Liu, T. Masese, H. Zhang and Y. Ma, *Chem. Eng. J.*, 2020, **387**, 124080.
37 J. Zhang, Z. Cao, L. Zhou, G. Park, L. Cavallo, L. Wang, H. N. Alshareef, Y. Sun and J. Ming, *ACS Energy Lett.*, 2020, **5**, 3124–3131.
38 V. Augustyn, J. Come, M. A. Lowe, J. W. Kim, P. Taberna, S. H. Tolbert, H. D. Abruña, P. Simon and B. Dunn, *Nat. Mater.*, 2013, **12**, 518–522.

